Monte Carlo study of the hull distribution for the $q = 1$ Brauer model

Wouter Kager* and Bernard Nienhuis

Instituut voor Theoretische Fysica
Valckenierstraat 65
1018 XE Amsterdam, the Netherlands

kager@eurandom.tue.nl, nienhuis@science.uva.nl

Abstract

We study a special case of the Brauer model in which every path of the model has weight $q = 1$. The model has been studied before as a solvable lattice model and can be viewed as a Lorentz lattice gas. The paths of the model are also called self-avoiding trails. We consider the model in a triangle with boundary conditions such that one of the trails must cross the triangle from a corner to the opposite side. Motivated by similarities between this model, SLE(6) and critical percolation, we investigate the distribution of the hull generated by this trail (the set of points on or surrounded by the trail) up to the hitting time of the side of the triangle opposite the starting point. Our Monte Carlo results are consistent with the hypothesis that for system size tending to infinity, the hull distribution is the same as that of a Brownian motion with perpendicular reflection on the boundary.

1 Introduction to the model

In this paper we present results from a Monte Carlo study of a special case of the Brauer model. This model has appeared in the literature in different guises, and received the name Brauer model only recently. Originally, it was studied as a q-state solvable vertex model [20] and later as an $\mathrm{O}(q)$ symmetric, solvable lattice model [18, 23]. More recently it was observed

*Present address: EURANDOM, P.O. Box 513, 5600 MB Eindhoven, the Netherlands

that the model could be seen as a model of paths on the lattice in which each closed path has a weight equal to q, where q can take non-integer values. In this language of paths each vertex can carry one of the following configurations of path segments, with the corresponding weights:

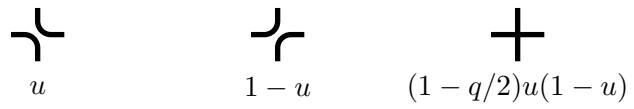

u $\qquad$ $1-u$ $\qquad$ $(1-q/2)u(1-u)$

Here the weights are chosen to be solutions of the Yang-Baxter (or star-triangle) equation [3, 4]. Although the integrability condition in the Yang-Baxter equation does not restrict q, the actual solution by means of the Bethe Ansatz was only extended to the integers [17].

The name Brauer model was given to emphasise that the transfer matrix of the model is an element of the Brauer algebra [8]. The model attracted particular attention in the limit $q \to 1$ when it describes the probability distribution of lattice paths taken by a particle that is scattered by randomly placed, static scatterers [9, 13, 19, 26]. As such it can be viewed as a Lorentz lattice gas, although in these applications the vertex weights are usually not chosen as above.

Another paradigm is coming from the analogy to the self-avoiding walk, as in the Brauer model a walk is not permitted to traverse a lattice edge more than once. A walk subject to this condition and with no further restrictions on the vertices is called a self-avoiding trail (SAT) [16]. We will therefore refer to the paths in the Brauer model as *trails*. Here we study the model at $q = 1$ on a bounded domain, and we will be interested in the distributions of special points on the boundary that are visited by one of the trails. This will be explained in more detail below.

First we introduce some notation. For given angles α and β in the range $(0, \pi)$ such that $\alpha + \beta < \pi$, we define $T_{\alpha,\beta}$ as the triangle in the upper half of the complex plane with vertices at 0 and 1, such that the interior angle at 0 is α and the interior angle at 1 is β. By $w_{\alpha,\beta}$ we will denote the third vertex of $T_{\alpha,\beta}$. For a given angle $\phi \in (0, \pi/2)$ and integer system size $N > 0$, let $V = V_\phi$ be the set of vertices $\{2j \cos\phi + k \exp(i\phi) : j, k \in \mathbb{N}, j + k \leq N\}$. Properly rescaled, this collection of vertices provides a nice covering of the isosceles triangle $T_{\phi,\phi}$ with base angle ϕ, see figure 1.

We define the Brauer model on V with $q = 1$ as follows. Each vertex of V can carry either of the three following configurations of trail segments:

$a =$  $\qquad$ $b =$  $\qquad$ $c =$

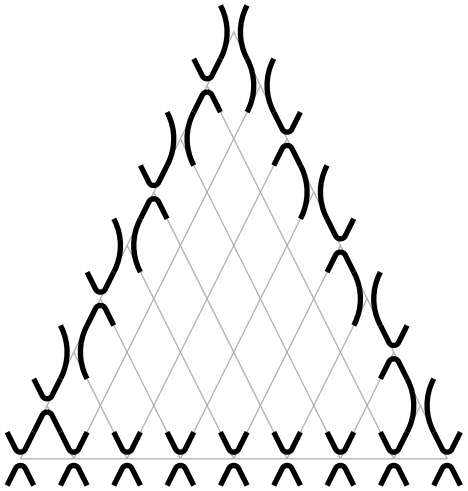

Figure 1: Boundary conditions for the self-avoiding trail in a triangle.

Here, the third vertex state should be interpreted as a crossing. The state of each vertex is chosen from $\{a, b, c\}$ independently from the states of the other vertices, with the probabilities for the three states given by

$$p(a) = \lambda\pi\, 2\phi \qquad p(b) = \lambda\pi\,(\pi - 2\phi) \qquad p(c) = \lambda\,\phi(\pi - 2\phi) \tag{1}$$

where $\lambda := [\pi^2 + \phi(\pi - 2\phi)]^{-1}$ provides the normalisation. Two distant edges may or may not be connected to each other by a trail. The correlations of these events are expected to be isotropic in space for large distances, if the weights are chosen as in equation (1) and vertices are arranged in space as in figure 1. The anisotropy of the weights is thus precisely compatible with the spatial anisotropy of the lattice, see [12].

Each configuration of vertex states defines a collection of self-avoiding trails on the vertex set V. We will be interested only in those configurations in which one of these trails crosses the triangular domain from a given corner to the opposite side. To make this trail stay inside the triangle we have to impose suitable boundary conditions. We choose the boundary conditions as shown in figure 1. Here it is assumed that the system size N is an even number, so that each side of the triangle carries an odd number of vertices. With these boundary conditions, one trail of the model must enter the triangle at the top or the lower-left corner, and stay inside the triangle until it leaves at the other of these two corners.

In our simulations we generate this particular self-avoiding trail dynamically as follows. Initially, only the vertex states on the boundary are fixed

according to the boundary conditions. The vertex states in the interior are still undecided. The trail starts from either the top or the lower-left corner of the triangle. The steps of the trail follow the trail segments of the vertex states. Each time the trail meets a vertex whose state is still undetermined, we choose its state according to the probabilities $p(a)$, $p(b)$ and $p(c)$ given above, and continue the random walk. The state of this vertex is fixed forever onwards. We stop the simulation as soon as the trail hits a vertex on the side of the triangle opposite the starting point.

We want to study the distribution of the point where the trail hits the side opposite the starting point in the limit when N becomes large. In fact, we are interested in the distribution of the so-called *hull* generated by the trail up to the stopping time, that is, the collection of points in the triangle that are disconnected by the stopped trail from the side of the triangle opposite the starting point. This will be motivated in more detail in section 2. As we shall explain, the main motivation for our study of the hull distribution is the close connection between the Brauer model and critical bond percolation, for which the hull distribution is known (although rigorously only for critical site percolation on the triangular lattice).

To make the connection with bond percolation, let us modify the model above by setting $p(c) = 0$, and let $p(a)$ and $p(b)$ be proportional to $\sin(2\phi/3)$ and $\sin((\pi - 2\phi)/3)$, respectively (see for instance [11, section 5]). For any given configuration of the model, one can draw at every vertex either the horizontal or the vertical edge connecting the centres of two adjacent rhombi (see figure 1), such that the drawn edge does not intersect a trail segment at that vertex. It is easy to see that the drawn edges constitute a configuration of bond percolation on a rectangular lattice together with the dual configuration. On the boundary we have a percolation cluster along the base and right side of the triangle and a dual cluster along the left side. Note that as before, there is one special path in the model that crosses the triangle between the top and the lower-left corner, and that this path describes the interface between the cluster and the dual cluster attached to the boundary. This path is called the percolation exploration process.

Thus we can interpret the Brauer model at $q = 1$ as a variant of a loop model for percolation with the added possibility that the loops may cross. Note that these crossings happen only with small probability, since $p(c)$ is the smallest of the three weights. One can therefore expect a self-avoiding trail to explore space much like the exploration process of critical percolation, except that occasionally the trail may cross and possibly re-enter a part of space it has already explored.

2 Conformal invariance and locality

In section 1 we introduced the Brauer model. It is believed that the scaling limit of this model is conformally invariant. Moreover, a self-avoiding trail of the model has the locality property. The purpose of this section is to explain what we precisely mean by these two properties, and to discuss an important implication.

To explain conformal invariance, suppose that for every domain in $\mathbb{C}$ with continuous boundary and suitable boundary conditions, we are given a probability measure on the collection of paths in that domain. Then we say that this family of measures (or the family of random paths they describe) is conformally invariant if for any conformal map g from a domain D onto a domain D' that maps corresponding boundary conditions onto each other, the image of the measure on paths in D by g coincides with the measure on paths in D'.

Now let T be a triangle in the upper half of the complex plane with vertices at 0, 1 and w, and suppose that D is of the form $T \setminus A$, where $A \subset T$ is such that $T \setminus A$ is simply connected and $w \in (\partial T \setminus \partial A)$, see figure 2. Let the map $g_A : T \to T \setminus A$ fix w and send $\partial T \setminus [0,1]$ onto the boundary arc B_A of $\partial T \setminus \partial A$ containing w. Consider a random path W in this triangle which starts in w and is stopped as soon as it hits the interval $[0,1]$. Then we say that W has the locality property if the path in T started from w and stopped at the first time when it hits $\partial D \setminus B_A$, has the same distribution as the path in D started from w and stopped on $\partial D \setminus B_A$. Note that if W is conformally invariant, then the latter random path is the image of the former by g_A.

For a local, conformally invariant path W in T, let τ denote the first time when W hits the interval $[0,1]$, and set $X := W(\tau)$. Then we define the *hull* K generated by the path as the set of points in $\overline{T}$ that are either on $W[0,\tau]$ or are disconnected from $\{0,1\}$ by $W[0,\tau]$. Observe that the distribution of this hull K is determined if we know for all sets A as in the previous paragraph the probability that $K \cap A = \emptyset$. But by the locality property, this probability is exactly the probability that the path W in $D = T \setminus A$ stopped when it hits $\partial D \setminus B_A$, is stopped in the interval $[0,1]$. Using conformal invariance, this probability equals the probability that X is in the interval $g_A^{-1}([0,1] \setminus \partial A)$, see figure 2. It follows that for local paths, the distribution of the hull K is determined by the distribution of the exit point X (see [24] for an illuminating discussion).

To examine some concrete examples, let T be an equilateral triangle (in other words, take $w = \exp(\mathrm{i}\pi/3)$). Then there are three known local and

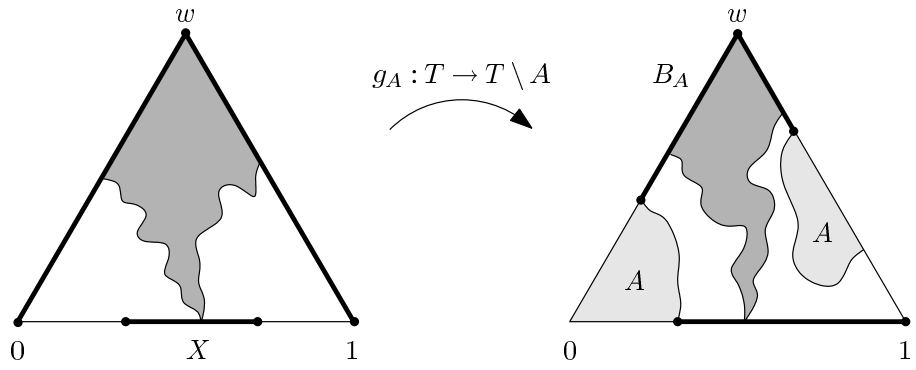

Figure 2: A hull generated by a local path in a triangle T. The distribution of the hull is determined by the probabilities that it avoids sets A such as shown on the right.

conformally invariant paths such that X has the uniform distribution. The first example is the trace of Schramm-Löwner Evolution (SLE) for $\kappa = 6$ [15, 25]. The second example is a Brownian motion in T which is reflected on the left side in the direction given by the vector $\exp(-\mathrm{i}\pi/3)$ and on the right side in the direction given by $\exp(-2\mathrm{i}\pi/3)$ [14, 25] (for details on reflected Brownian motion, see section 3). The third example is the scaling limit of the exploration process for critical site percolation on the triangular lattice in T [21]. Since the distribution of X is the same for these paths, by the result of the previous paragraph they generate hulls K with the same distribution.

As we explained in section 1, the Brauer model studied here is closely related to critical percolation. One may therefore expect the distribution of the hull to be the same for the two models. This can be motivated further by the fact that any two local and conformally invariant processes in the plane which are started in the origin and stopped upon hitting the unit circle generate the same hull, namely that of a stopped Brownian motion (see [24]). In a bounded domain, however, our Monte Carlo study shows that the hull distributions for critical percolation and for the Brauer model are not the same. Instead, one of the results of this paper is that our numerical data are consistent with the hypothesis that in the scaling limit, the hull of the Brauer model has the same distribution as that of a Brownian motion which is reflected perpendicularly on the boundary of the domain.

To study the distribution of the hull for the Brauer model, by locality it is in principle sufficient to look only at the distribution of the exit point X

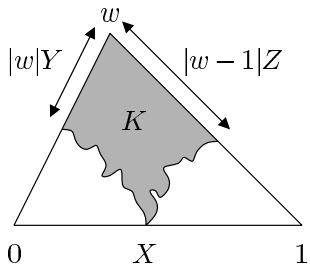

Figure 3: Definition of the hull K of a local path in the triangle T, and of the random variables X, Y and Z.

in a given triangle. However, for obvious reasons we prefer to consider more characteristics of the hull. For this purpose we introduce two new random variables Y and Z associated with the hull K in the triangle T, as follows. We shall denote by $|w|Y$ the distance of the lowest point of the hull on the left side of T to the top w, and by $|w-1|Z$ the distance of the lowest point of the hull on the right side to the top w. Thus, all three random variables X, Y and Z take values in the range $[0,1]$. See figure 3 for an illustration.

In section 3 we shall compute the (joint) distributions of X, Y and Z for the case of reflected Brownian motion. These distributions can then be compared with the corresponding distributions in the Brauer model. The results of our Monte Carlo study of the hull distribution are discussed in section 4. In section 5 we present simulation results for a different distribution, the last-visit distribution.

3 Reflected Brownian motion

In this section we define reflected Brownian motion in triangles and summarize the main results on these processes. We recall that for given angles λ and μ in the range $(0,\pi)$ such that $\lambda+\mu<\pi$, we define $T=T_{\lambda,\mu}$ as the triangle in the upper half of the complex plane with vertices at 0 and 1, such that the interior angle at 0 is λ and the interior angle at 1 is μ. By $w=w_{\lambda,\mu}$ we denote the third vertex of $T_{\lambda,\mu}$.

Let us now introduce the (reflection) angles $\alpha,\beta\in(0,\pi)$ and set $v_L:=\exp(\mathrm{i}(\lambda+\alpha-\pi))$, $v_R:=\exp(-\mathrm{i}(\mu+\beta))$. We want to consider a stochastic process Z in T which is Brownian motion in the interior, and which is reflected instantaneously in the direction given by v_L or v_R when it hits the left or right side of T, respectively. Such a process is called a reflected

Brownian motion with reflection vector fields v_L and v_R on the sides of T. We write $\mathrm{RBM}_{\alpha,\beta}$ to denote this process. Note that the angles α and β are the reflection angles measured with respect to the boundary.

More explicitly, an $\mathrm{RBM}_{\alpha,\beta}$ in T may be defined as follows. Let B be standard two-dimensional Brownian motion. Then an $\mathrm{RBM}_{\alpha,\beta}$ in T is the unique process Z such that

$$Z(t) = B(t) + v_L\, Y_L(t) + v_R\, Y_R(t), \tag{2}$$

where Y_L, Y_R are continuous increasing real-valued processes adapted to B which satisfy $Y_L(0) = Y_R(0) = 0$ and increase only when Z is on the left, respectively right, side of T [22, equation (2.4)]. This process is well-defined up to the first time when Z hits the interval $[0, 1]$. For a characterisation and properties of these reflected Brownian motions, see Varadhan and Williams [22]. It is straightforward to show conformal invariance and locality for these processes, see for instance [25, chapter 5].

It was shown by Lawler et al. [15] that if we take an $\mathrm{RBM}_{\pi/3,\pi/3}$ in the equilateral triangle $T_{\pi/3,\pi/3}$, then the exit distribution is uniform. Their arguments were generalised to isosceles triangles (i.e. the triangles $T_{\lambda,\lambda}$) by Dubédat [6], and then to the case of a generic triangle (any $T_{\lambda,\mu}$ such that $\lambda + \mu < \pi$, with a natural extension to the case $\lambda + \mu \geq \pi$) by one of us [10]. These results show that an $\mathrm{RBM}_{\alpha,\beta}$ in the triangle $T_{\alpha,\beta}$ has the uniform exit distribution. By conformal invariance, this also determines the exit distribution for an $\mathrm{RBM}_{\alpha,\beta}$ in any triangle $T_{\lambda,\mu}$, and using locality we can in fact compute the joint distribution of the exit point X and the lowest points Y and Z of the hull on the two sides, as we show next.

It turns out that the distributions of the random variables X, Y and Z can all be expressed in terms of conformal transformations of the upper half-plane onto triangles $T_{\gamma,\delta}$. By the Schwarz-Christoffel formula [1], the unique conformal transformation of the upper half-plane onto $T_{\gamma,\delta}$ that fixes 0 and 1 and maps ∞ to $w_{\gamma,\delta}$ is given by

$$F_{\gamma,\delta}(z) = \frac{\int_0^z t^{\gamma/\pi-1}(1-t)^{\delta/\pi-1}\mathrm{d}t}{\int_0^1 t^{\gamma/\pi-1}(1-t)^{\delta/\pi-1}\mathrm{d}t}\,. \tag{3}$$

By the substitution $t \mapsto 1 - u$ it is easy to show that

$$F_{\gamma,\delta}(z) = 1 - F_{\delta,\gamma}(1-z) \quad \text{and} \quad F^{-1}_{\gamma,\delta}(z) = 1 - F^{-1}_{\delta,\gamma}(1-z). \tag{4}$$

We shall now explain how we can express the distribution functions for X, Y and Z in terms of these conformal transformations.

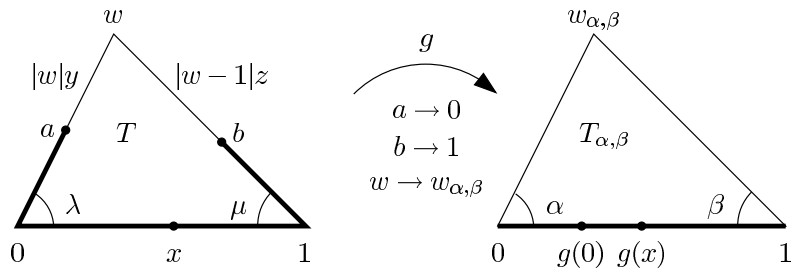

Figure 4: This figure illustrates how the joint distribution function of the random variables X, Y and Z can be computed. As explained in the text, the joint probability $\mathbf{P}[X \leq x, Y \leq y, Z \leq z]$ is just $g(x) - g(0)$.

The idea of the computation of $\mathbf{P}[X \leq x, Y \leq y, Z \leq z]$ is illustrated in figure 4. Consider an $\mathrm{RBM}_{\alpha,\beta}$ in the triangle $T = T_{\lambda,\mu}$ started from the top $w = w_{\lambda,\mu}$. Let $a = a(y)$ and $b = b(z)$ be the points on the left and right sides of T at distances $|w|y$ and $|w-1|z$ from w, respectively. Stop the RBM as soon as it hits the counter-clockwise arc from a to b on the boundary (the thick line in figure 4). Then the probability $\mathbf{P}[X \leq x, Y \leq y, Z \leq z]$ is just the probability that this process is stopped in the interval $(0, x)$.

We now use conformal invariance and locality. Let $g = g_{a(y),b(z)}$ be the conformal map of T onto $T_{\alpha,\beta}$ that sends a to 0, b to 1 and w to $w_{\alpha,\beta}$, as illustrated in figure 4. Then we are looking for the probability that an $\mathrm{RBM}_{\alpha,\beta}$ in $T_{\alpha,\beta}$ started from $w_{\alpha,\beta}$ and stopped when it hits $[0, 1]$, is stopped in the interval $(g(0), g(x))$. But since the exit distribution of the $\mathrm{RBM}_{\alpha,\beta}$ is uniform in $T_{\alpha,\beta}$, this probability is simply $g(x) - g(0)$. Thus,

$$\mathbf{P}[X \leq x, Y \leq y, Z \leq z] = g(x) - g(0). \tag{5}$$

It remains to find an explicit form of the map $g = g_{a(y),b(z)}$. At this point it is useful to denote by ν the third angle of the triangle $T_{\lambda,\mu}$, that is, $\nu := \pi - \lambda - \mu$. The explicit form of g can be obtained by suitably combining conformal self-maps of the upper half-plane with triangle mappings. How this is done exactly is described in figure 5.

By studying this figure we obtain the formula

$$\mathbf{P}[X \leq x, Y \leq y, Z \leq z] = F_{\alpha,\beta}\left(\frac{F^{-1}_{\lambda,\mu}(x) - F^{-1}_{\lambda,\mu}(a)}{F^{-1}_{\lambda,\mu}(b) - F^{-1}_{\lambda,\mu}(a)}\right) - F_{\alpha,\beta}\left(\frac{-F^{-1}_{\lambda,\mu}(a)}{F^{-1}_{\lambda,\mu}(b) - F^{-1}_{\lambda,\mu}(a)}\right) \tag{6}$$

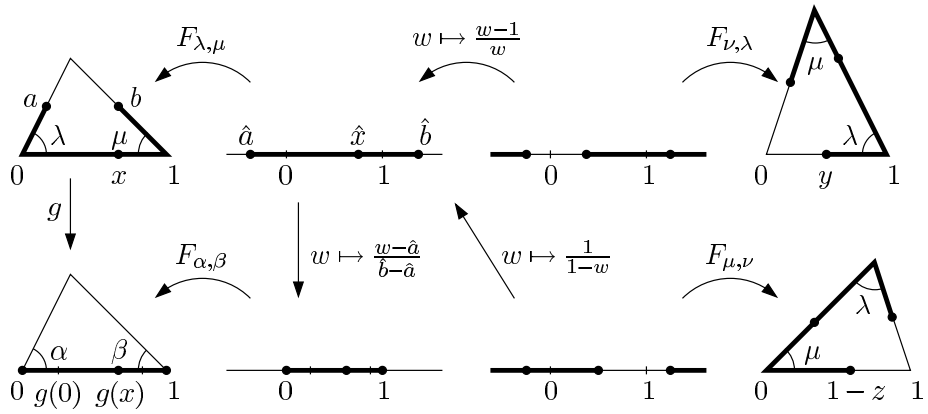

Figure 5: This illustration shows schematically how one obtains an explicit form for the map g in terms of the variables y and z. The notations $\hat{a}$, $\hat{b}$ and $\hat{x}$ in the figure are short for $F_{\lambda,\mu}^{-1}(a)$, $F_{\lambda,\mu}^{-1}(b)$ and $F_{\lambda,\mu}^{-1}(x)$.

where the images of a and b under $F_{\lambda,\mu}^{-1}$ can be expressed in terms of y and z as

$$F_{\lambda,\mu}^{-1}(a) = 1 - \frac{1}{F_{\nu,\lambda}^{-1}(y)}\,; \qquad F_{\lambda,\mu}^{-1}(b) = \frac{1}{1 - F_{\mu,\nu}^{-1}(1-z)} = \frac{1}{F_{\nu,\mu}^{-1}(z)}\,. \tag{7}$$

Sending two of the variables x, y, z to 1 and using the symmetry property (4) of the triangle mappings, we obtain

$$\mathbf{P}[X \le x] = F_{\alpha,\beta}\big(F_{\lambda,\mu}^{-1}(x)\big); \tag{8}$$

$$\mathbf{P}[Y \le y] = F_{\beta,\alpha}\big(F_{\nu,\lambda}^{-1}(y)\big); \tag{9}$$

$$\mathbf{P}[Z \le z] = F_{\alpha,\beta}\big(F_{\nu,\mu}^{-1}(z)\big). \tag{10}$$

Observe that these three distributions have particularly simple forms with a nice geometric interpretation. For instance, $\mathbf{P}[Y \le y]$ is just the image of y under the transformation that maps the triangle $T_{\nu,\lambda}$ onto $T_{\beta,\alpha}$, fixes 0 and 1 and takes $w_{\nu,\lambda}$ onto $w_{\beta,\alpha}$.

4 Hull distribution of the Brauer model

We now return to the Brauer model introduced in section 1. To compare the hull of the model with the hull of reflected Brownian motion, we measure the (joint) distributions of the random variables X, Y and Z (introduced in

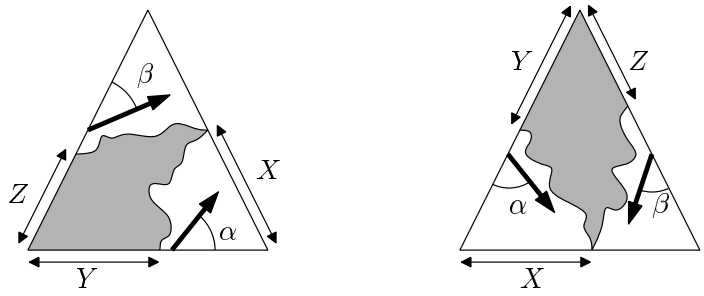

Figure 6: How the random variables X, Y and Z and reflection angles α and β are associated to the trails starting from different corners. For simplicity we have omitted the normalisation of X, Y and Z.

section 2) in our simulations of the Brauer model. The data are collected for 10^6 independent trails starting from the top and 10^6 independent trails starting from the lower-left corner on the set of vertices $V = V_\phi$ for the 12 different system sizes $N = 100$, 200, 300, 400, 600, 800, 1200, 1600, 2000, 2400, 3200, 4000 and 8 different base angles ϕ ranging from 10° up to 80° with 10° intervals. Below we shall describe more precisely how the data for the (joint) distributions of X, Y and Z are collected.

We distribute the vertices of V on the three sides of the triangle over a total of 100 bins, each containing $N/100$ vertices. Since there are actually $N + 1$ vertices on each side, this means that one vertex on each side is omitted. This is the vertex in the corner of the side where the associated random variable X, Y or Z is 0. In the simulations we record the number of trails X_i that land in the ith bin for each $i = 1, 2, \ldots, 100$. We also record the numbers of walks Y_i, respectively Z_i, such that the ith bin on the right, respectively left, side of the triangle (as seen from the starting point) is the bin furthest from the starting point which was visited by the trail. Figure 6 illustrates how the variables X, Y and Z are associated with the hulls of trails starting from different corners. The joint distributions of these variables are recorded similarly, but instead of using 100 bins on the sides we use 50 bins to reduce memory requirements.

In this way the simulations build up histograms of the marginal and joint distributions of X, Y and Z for the self-avoiding trail that can be compared to the corresponding distributions for the reflected Brownian motions. To improve the statistics, we first merge together bins of collected data in order to distribute the numbers of trails in different bins more evenly. We shall explain below how this merging procedure works for the joint distribution

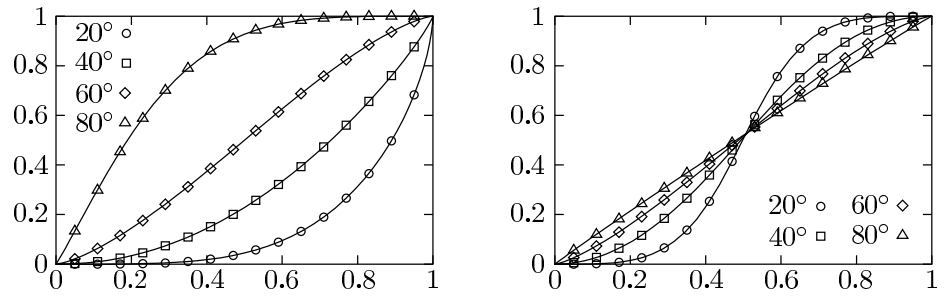

Figure 7: The distribution functions $\mathbf{P}[X \leq x]$ (left) and $\mathbf{P}[Y \leq y]$ (right) for the self-avoiding trail on different triangles with system size $N = 4000$, started from the lower-left corner. The solid lines are the corresponding distributions for a reflected Brownian motion for which we obtain an optimal least-squares fit. See table 1 for the corresponding values of α and β.

of X, Y and Z. A similar procedure is applied for the joint distributions of two of the three random variables and for the marginal distributions.

For the joint distribution of X, Y and Z, from our simulations we have a total of $50 \times 50 \times 50$ cubical bins that span the unit cube with the variables X, Y and Z along the axes. We consider merging together either $10 \times 10 \times 10$, or $5 \times 5 \times 5$, or $2 \times 2 \times 2$ of these cubical bins into larger cubical bins, that together with the unmerged bins form a partition of the unit cube. Our aim is that each bin in the final partition of the unit cube represents at least 100 generated trails, 0.01% of the total. Moreover, we want each bin that represents at least 1% (10^4) of the total number of generated trails to be present in the final partition.

The merging procedure therefore works as follows. First, we consider for each of the $10 \times 10 \times 10$ cubes whether it should form a large bin, or be built up from smaller bins. So we do the following test: if we would built it up from $2 \times 2 \times 2$ bins, then would each constituting bin contain at least 100 trails, or would one of these bins contain at least 10^4 trails? If so, the $10 \times 10 \times 10$ cube is split into $2 \times 2 \times 2$ cubes. Then we test whether each of these $2 \times 2 \times 2$ cubes should form a bin, or be built up from $1 \times 1 \times 1$ bins, by the same criterion as above. Otherwise, we test whether the $10 \times 10 \times 10$ cube can be built up from $5 \times 5 \times 5$ (rather than $2 \times 2 \times 2$) cubes. If so, we test whether each of these $5 \times 5 \times 5$ cubes should form a bin, or be built up from $1 \times 1 \times 1$ bins, as before. In the end, we achieve a more even distribution of trails over a smaller number of bins, as desired.

As we explained, we want to compare the distribution of the hull gener-

	20°		40°		60°		80°	
	α/π	β/π	α/π	β/π	α/π	β/π	α/π	β/π
X	0.456(1)	0.484(2)	0.461(2)	0.474(2)	0.464(2)	0.464(2)	0.464(2)	0.453(2)
Y	0.456(1)	0.446(1)	0.462(2)	0.445(1)	0.464(1)	0.438(2)	0.461(2)	0.431(2)
Z	0.447(2)	0.483(2)	0.445(1)	0.475(2)	0.439(2)	0.464(2)	0.431(1)	0.452(1)

Table 1: Fitted values for α and β on different triangles compared for the different marginal distributions of X, Y and Z (system size $N = 4000$, trails start from the lower-left corner).

ated by the trails with the hull distribution of reflected Brownian motion, in particular in the limit when the system size becomes large. Our working hypothesis is therefore that the binned data collected in the simulations is predicted by the joint distribution function (6) for the RBM with parameters α, β for some α and β as $N \to \infty$. To test this hypothesis, we make a least-squares fit of the parameters α and β for each system size N. For every triangle $T_{\phi,\phi}$ on which we have simulated the model and for each of the two possible starting points, this gives us a list of the best-fit values for α and β for 12 different system sizes. We want to investigate whether these values of α and β converge to a common limit as the system size becomes larger and larger.

The least-squares fits show that the marginal distributions of X, Y and Z for the self-avoiding trail are well described by those of an RBM (see figure 7). More precisely, as the system size N gets larger, the value of χ^2 (the difference between the actual and the predicted number of walks in each bin squared, divided by the predicted variance in this number, summed over all the bins) goes down to a value close to the number of bins, see for instance table 2. However, the fitted values we obtain for α and β are not constant with the system size. More work is therefore needed to test convergence of α and β to a limit as $N \to \infty$.

We also observe from the simulations that the fitted values of α and β for the three distributions of X, Y and Z do not fully agree. It seems that the fitted values of α do agree for the distributions of X and Y, whereas the fitted values of β do agree for the distributions of X and Z. The fitted value of α for the distribution of Z agrees with the fitted value of β for the distribution of Y. See table 1. This observation holds both for trails starting from the top of the triangle and for trails starting from the lower-left corner at different system sizes. This is another indication that more work is required to test convergence of α and β as $N \to \infty$.

Interestingly, for trails that start in the lower-left corner of an *equilateral*

triangle the fitted values of α and β *do* agree for the exit distribution at different system sizes (see table 2). In other words, the exit distribution of the trails is symmetric in an equilateral triangle. Note that this result is not trivial because our boundary conditions are not symmetric between the left side and the base of the triangle, see figure 1. We infer that our choice of boundary conditions does not destroy the isotropy of the model, and hence does not interfere with conformal invariance in the scaling limit.

Before we consider the convergence to a limit in more detail, let us also consider the joint distributions of X, Y and Z. Since the fits of the marginal distributions give different values of α and β at finite system sizes, it is to be expected that the joint distributions measured in the simulations will not be well described by those of an RBM. This is indeed what we see when we try to fit the data for the joint distributions to the distribution function for the RBMs, see for instance table 2. We note that the value of χ^2 for the fits of the joint distributions is several times the number of bins at small system sizes. However, χ^2 does go down as the system size increases, which is a sign that the fits become better for larger systems.

If the hull of the self-avoiding trail does converge to that of a reflected Brownian motion in the scaling limit, then the fitted values of α and β should converge to a limit value as $N \to \infty$. From the change in the fitted values of α and β with system size observed in the simulations we can see that if there is convergence, then it is very slow. We make the educated guess that α and β converge with the system size N as $1/\log_{10} N$ (corrections that behave as a power of $\log_{10} N$ rather than as a power of N itself are consistent with earlier findings [17] and with the presence of a zero conformal weight).

To test convergence, we therefore make a linear fit of the fitted values of α and β for the different distributions on different triangles against $1/\log_{10} N$. We accept the linear fit if it passes each of the following three tests:

1. We look at the value of χ^2 for the fit. If this value exceeds the 10% probability threshold for the χ^2 distribution, we reject the fit.

2. We compare the value of the intercept at $N = \infty$ from the linear fit with the value we obtain if we fit the data to a parabola in $1/\log_{10} N$. If the values do not agree within 1.96 standard deviation (the Gaussian 5% level) of the linear fit, the fit is rejected.

3. We do a run test. If the data is well described by a line, then each data point should be independently above or below this line with equal probabilities. Thus we can predict how many consecutive runs of

	Marginal distribution of X				Joint distribution of X, Y and Z			
N	α/π	β/π	χ^2	#bins	α/π	β/π	χ^2	#bins
100	0.421(5)	0.439(5)	7754	99	0.428(4)	0.434(3)	8401	1193
200	0.440(2)	0.449(2)	556	100	0.436(4)	0.441(3)	8577	1317
300	0.445(3)	0.450(3)	708	100	0.440(4)	0.443(4)	8375	1207
400	0.448(2)	0.452(2)	311	100	0.442(4)	0.444(5)	8386	1193
600	0.453(2)	0.455(2)	238	100	0.445(4)	0.447(4)	8181	1200
800	0.454(2)	0.457(2)	201	100	0.448(4)	0.450(3)	8280	1310
1200	0.457(2)	0.458(2)	148	100	0.451(4)	0.452(4)	7661	1427
1600	0.460(2)	0.461(2)	160	100	0.453(4)	0.454(4)	7938	1441
2000	0.460(1)	0.461(2)	123	100	0.453(4)	0.454(4)	7392	1200
2400	0.461(2)	0.462(1)	110	100	0.455(4)	0.455(4)	7102	1083
3200	0.462(2)	0.462(2)	152	100	0.455(4)	0.456(3)	7228	1317
4000	0.464(2)	0.464(2)	126	100	0.457(3)	0.457(3)	7118	1434

Table 2: Fitted values for α and β together with the value of χ^2 and the number of bins for two different distributions of a trail on an equilateral triangle, started from the lower-left corner.

points above the line and below the line to expect. If the probability for the number of runs we find is less than 12%, the fit is rejected.

For more background on these (and other) kinds of tests for data fitting, the reader can consult for instance Barlow [2].

We have a total of 224 sets of data points for which we attempt a linear fit (3 marginal distributions plus 4 joint distributions for the variables X, Y and Z, times 8 different base angles, times 2 because the trails can start either from the top or the lower-left corner, times 2 variables α and β). Of these, 39 (17%) give an accepted linear fit in the 12 system sizes, and an additional 27 (for a total of 66, i.e. 29%) give an accepted linear fit if we leave out the smallest system size. For the other sets of data we can not observe the convergence from our simulations without further knowledge of how α and β should behave as functions of N.

From each accepted linear fit of α or β against $1/\log_{10} N$ we obtain a value for the intercept with the α- or β-axis as $N \to \infty$. Considering only the accepted linear fits with all 12 system sizes taken into account, these intercept values give $\alpha/\pi \to 0.4964(48)$ and $\beta/\pi \to 0.4952(75)$ as $N \to \infty$. If we include the additional accepted linear fits where the smallest system size is left out, we obtain $\alpha/\pi \to 0.4955(54)$ and $\beta/\pi \to 0.4952(66)$. These results are consistent with the hypothesis that the hull of the self-avoiding trail in the scaling limit is the same as that of an $\mathrm{RBM}_{\pi/2,\pi/2}$, that is, a reflected Brownian motion with perpendicular reflection on the boundary.

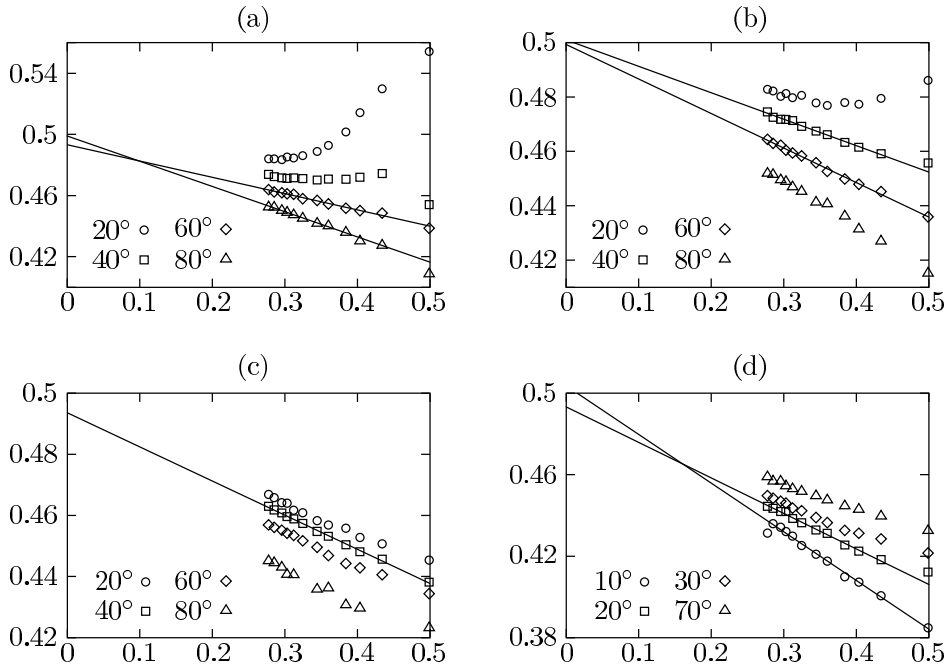

Figure 8: Graphs (a), (b) and (c) show the fitted values of β/π against $1/\log_{10} N$ for the marginal distributions of X and Z and the joint distribution of X, Y and Z, respectively, for trails started from the left corner. Graph (d) shows the fitted values of α/π against $1/\log_{10} N$ for the joint distribution of X, Y and Z for trails started from the top. In those cases where a linear fit is accepted, the fitted line is shown as well.

5 Percolation and the last-visit distribution

In this section we look at a different distribution for the self-avoiding trail of the Brauer model. The motivation for this comes from a further connection between the percolation exploration process and $\mathrm{RBM}_{\pi/3,\pi/3}$ discovered by Dubédat [7], the analogue of which we want to investigate for the Brauer model. But first let us consider the case of percolation. In section 1 we explained that the Brauer model studied in this paper becomes a model for critical bond percolation if we take the probabilities of the vertex states a and b on page 2 proportional to $\sin(2\phi/3)$ and $\sin((\pi-2\phi)/3)$, respectively, and $p(c)=0$. The paths defined by the model then correspond to the boundaries of the percolation clusters, or equivalently, to a percolation exploration process. The hull generated by a path of the model should therefore have

		from the top		from the left corner	
	angle	α/π	β/π	α/π	β/π
joint distribution	20°	0.331(4)	0.350(4)	0.334(2)	0.334(2)
	40°	0.334(4)	0.339(3)	0.333(1)	0.334(2)
	60°	0.334(2)	0.333(1)	0.333(2)	0.335(2)
	80°	0.333(1)	0.331(1)	0.331(2)	0.335(2)
last-visit distribution	20°	0.336(2)	0.335(2)	0.332(2)	0.329(3)
	40°	0.329(4)	0.331(3)	0.332(3)	0.332(2)
	60°	0.332(3)	0.334(3)	0.332(3)	0.332(3)
	80°	0.328(4)	0.339(3)	0.327(3)	0.333(3)

Table 3: Fitted values for α and β on different triangles for the joint and last-visit distributions of the exploration process of critical bond percolation at system size $N = 2000$.

the same distribution as the hull of an $\mathrm{RBM}_{\pi/3,\pi/3}$ in the scaling limit, as we discussed in section 2.

Similar simulations as for the self-avoiding trails allow us to test this hypothesis. We have measured in the same way as before the joint distribution of the variables X, Y and Z on different triangles with fixed system size $N = 2000$. Our hypothesis is that this joint distribution is predicted by equation (6) for reflected Brownian motion with reflection angles α and β, where α and β should be equal to $\pi/3$. Table 3 shows the results of a least-squares fit for the reflection angles α and β, which agree with the hypothesis that the hull distribution is the same as that of an $\mathrm{RBM}_{\pi/3,\pi/3}$.

It was shown by Dubédat [7] that there exists a rather surprising further connection between reflected Brownian motion and the exploration process of critical percolation. To explain this connection, suppose that W is a local process in the triangle $T = T_{\lambda,\mu}$ started from $w = w_{\lambda,\mu}$, where λ, μ are fixed angles such that $\lambda + \mu < \pi$. Let $\tau := \inf\{t \geq 0 : W(t) \in [0,1]\}$, and let σ be the last time before τ when W visits the boundary of T. Let E denote the event that $W(\sigma)$ is on the right side of the triangle. Then we can consider the probability of the event E conditioned on $\{W(\tau) = x\}$. We call this conditional probability, which is a function of x, the *last-visit distribution* of W in T.

For reflected Brownian motion this last-visit distribution can be computed using the fact that the exit distribution is uniform in a well-chosen triangle. For the case of an $\mathrm{RBM}_{\pi/3,\pi/3}$ in an equilateral triangle, this computation was done by Dubédat in [6]. The generalization to an $\mathrm{RBM}_{\alpha,\beta}$ in

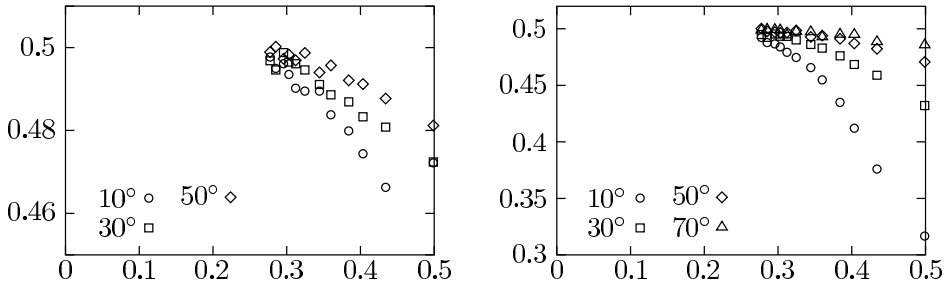

Figure 9: Fitted values of α/π (left) and β/π (right) plotted against $1/\log_{10} N$ for the last-visit distribution of trails starting from the lower-left corner of different triangles.

the triangle $T_{\lambda,\mu}$ started from $w_{\lambda,\mu}$ is straightforward, and gives

$$\mathbf{P}[E \mid W(\tau) = x] = F_{\pi-\alpha,\pi-\beta}\left(F^{-1}_{\lambda,\mu}(x)\right), \tag{11}$$

where $F_{\gamma,\delta}$, given by equation (3), is the unique conformal transformation of the upper half-plane onto $T_{\gamma,\delta}$ which fixes 0 and 1 and sends ∞ to $w_{\gamma,\delta}$.

The last-visit distribution can also be computed rigorously for chordal SLE(6), as was shown by Dubédat [7]. The obtained formula is exactly the formula (11) in the case of an $\mathrm{RBM}_{\pi/3,\pi/3}$ (i.e. $\alpha = \beta = \pi/3$). This fact is rather surprising if one considers the very different ways in which the two processes explore space: whereas an SLE(6) process never crosses itself, an $\mathrm{RBM}_{\pi/3,\pi/3}$ crosses itself many times. In particular, it is known that on the event E, the last point visited on the right side of the triangle T by an SLE(6) process must be also the lowest point of the hull on the right side. For an $\mathrm{RBM}_{\pi/3,\pi/3}$, however, the last point visited on the right side is almost surely not the lowest point of the hull.

Let us now return to our simulations of the exploration path of critical percolation. It is quite easy to count in these simulations the number of paths that land in a given bin and visited the side to the left (and not to the right) of the starting point last before reaching the opposite side. Divided by the total number of paths that land in a given bin, this binned data can be compared to the last-visit distribution of equation (11). Note, however, that this binned data represents the conditional probability of E given that the path lands in an interval rather than at a given point x. To make the comparison we therefore have to integrate (11) with respect to the exit distribution of the exploration path.

We take the exit distribution for the paths in the simulations to be well described by the least-squares fit for the marginal distribution of X. Then we can integrate (11) numerically (with α and β as parameters) with respect to this fixed exit distribution, and obtain from this the probability of E conditioned on the event that the path lands in a given bin. This can be used to make a least-squares fit for the parameters α and β of the last-visit distribution. Table 3 shows that our simulations for critical percolation are in agreement with the fact that the last-visit distribution is given by that of an $\mathrm{RBM}_{\pi/3,\pi/3}$.

A similar analysis can be carried out for the self-avoiding trails of the Brauer model. As before, here we face the problem that the model converges only slowly. We therefore make least-squares fits of α and β for different system sizes, and plot the results against $1/\log_{10} N$, see figure 9. It is clear that here we can not conclude what the scaling limit is, without an analytic prediction of how the parameters α and β behave as functions of N. However, our results do not exclude the possibility that the last-visit distribution for the self-avoiding trails in the scaling limit is the same as that of an $\mathrm{RBM}_{\pi/2,\pi/2}$, just like the distribution of the hull.

Conclusions We have carried out a classical Monte Carlo study of the hull distribution for the Brauer model at $q = 1$. Our results are in agreement with the hypothesis that the hull distribution coincides with that of a reflected Brownian motion with perpendicular reflection. We have tested our methods for percolation, and found good agreement with the fact that in this case the hull must have the same distribution as that of a Brownian motion which is reflected at angles of 60° with respect to the boundary. We have also studied the last-visit distribution, but for the Brauer model our simulation results are inconclusive.

Acknowledgements We thank Wendelin Werner for useful discussions in the early stages of this project. This work is part of the research programme of the 'Stichting voor Fundamenteel Onderzoek der Materie (FOM)', which is financially supported by the 'Nederlandse Organisatie voor Wetenschappelijk Onderzoek (NWO)'.

References

[1] Ahlfors, L. V. (1966, 2nd edition). *Complex analysis: an introduction to the theory of analytic functions of one complex variable*. New York:

McGraw-Hill.

[2] Barlow, R. J. (1989). *Statistics. A guide to the use of statistical methods in the physical sciences*. Chichester: John Wiley & Sons.

[3] Baxter, R. J. (1978). Solvable eight-vertex model on an arbitrary planar lattice. *Philos. Trans. Roy. Soc. London Ser. A 289*, pp. 315–346.

[4] Baxter, R. J. (1982). *Exactly solved models in statistical mechanics*. London: Academic Press.

[5] Camia, F. & Newman, C. M. (preprint). The full scaling limit of two-dimensional critical percolation. [math.PR/0504036].

[6] Dubédat, J. (2004). Reflected planar Brownian motions, intertwining relations and crossing probabilities. *Ann. Inst. H. Poincaré Probab. Statist. 40*, pp. 539–552. [math.PR/0302250].

[7] Dubédat, J. (preprint). Excursion decompositions for SLE and Watts' crossing formula. [math.PR/0405074].

[8] Gier, J. de & Nienhuis, B. (2005). Brauer loops and the commuting variety. *J. Stat. Mech. Theory Exp.* 006, 10 pp.

[9] Gunn, J. M. F. & Ortuño, M. (1985). Percolation and motion in a simple random environment. *J. Phys. A 18*, pp. L1095–L1101.

[10] Kager, W. (preprint). Reflected Brownian motion in generic triangles and wedges. Submitted to *Stoch. Process. Appl.* [math.PR/0410007].

[11] Kenyon, R. (preprint). An introduction to the dimer model. [math.CO/0310326].

[12] Kim, D. & Pearce, P. A. (1987). Scaling dimensions and conformal anomaly in anisotropic lattice spin models. *J. Phys. A 20*, pp. L451–L456.

[13] Kong, X. P. & Cohen, E. G. D. (1989). Anomalous diffusion in a lattice-gas wind-tree model. *Phys. Rev. B 40*, pp. 4838–4845.

[14] Lawler, G. F., Schramm, O. & Werner, W. (2001). Values of Brownian intersection exponents I: Half-plane exponents. *Acta Math. 187*, pp. 237–273. [math.PR/9911084].

[15] Lawler, G. F., Schramm, O. & Werner, W. (2003). Conformal restriction: the chordal case. *J. Amer. Math. Soc. 16*, pp. 917–955. [math.PR/0209343].

[16] Lyklema, J. W. (1985). The growing self-avoiding trail. *J. Phys. A* pp. L617–L624.

[17] Martins, M. J., Nienhuis, B. & Rietman, R. (1998). Intersecting loop model as a solvable super spin chain. *Phys. Rev. Lett. 81*, pp. 504–507.

[18] Reshetikhin, N. Y. (1983). The functional equation method in the theory of exactly soluble quantum systems. *Sovjet Phys. JETP 57*, pp. 691–696.

[19] Ruijgrok, T. W. & Cohen, E. G. D. (1988). Deterministic lattice gas models. *Phys. Lett. A 133*, pp. 415–418.

[20] Schultz, C. L. (1981). Solvable q-state models in lattice statistics and Quantum Field Theory. *Phys. Rev. Lett. 46*, pp. 629–632.

[21] Smirnov, S. (2001). Critical percolation in the plane: conformal invariance, Cardy's formula, scaling limits. *C. R. Acad. Sci. Paris Sér. I Math. 333*, pp. 239–244.

[22] Varadhan, S. R. S. & Williams, R. J. (1985). Brownian motion in a wedge with oblique reflection. *Comm. Pure App. Math. 38*, pp. 405–443.

[23] Vega, H. J. de & Karowski, M. (1987). Exact Bethe Ansatz solution of O($2n$) symmetric theories. *Nucl. Phys. B 280*, pp. 225–254.

[24] W. Werner (2001). Critical exponents, conformal invariance and planar Brownian motion. In: C. Casacuberta, R.M. Miro-Roig, J. Verdera and S. Xambo-Descamps, eds., *European Congress of Mathematics, Vol. II (Barcelona, 2000)*, pp. 87–103, *Progr. Math.* **202**. Basel: Birkhäuser, [arXiv:math.PR/0007042].

[25] Werner, W. (2004). Random planar curves and Schramm-Loewner evolutions. In *Lectures on probability theory and statistics*, vol. 1840 of *Lecture notes in Math.*, pp. 107–195. Berlin: Springer. [math.PR/0303354].

[26] Ziff, R. M., Kong, X. P. & Cohen, E. G. D. (1991). Lorentz lattice-gas and kinetic-walk model. *Phys. Rev. A 44*, pp. 2410–2428.